J. Fluid Mech. (1981), *vol.* 108, *pp.* 317–343
Printed in Great Britain

Simultaneous temperature and velocity measurements in the plane of symmetry of a transitional turbulent spot

By R. A. ANTONIA, A. J. CHAMBERS,

Department of Mechanical Engineering,
University of Newcastle, N.S.W., 2308, Australia

M. SOKOLOV

School of Engineering,
Tel Aviv University, Tel Aviv, 69978, Israel

AND C. W. VAN ATTA

Department of Applied Mechanics and Engineering Sciences,
University of California at San Diego, La Jolla, 92093, U.S.A.

(Received 5 April 1979 and in revised form 17 July 1980)

Simultaneous measurements of the longitudinal velocity U, normal velocity V, and temperature T have been made in turbulent spots generated in a slightly heated laminar boundary layer. The measurements were made in the plane of symmetry of the spot at several streamwise stations downstream of the spot-producing spark. Ensemble averages of U, V and T, obtained relative to the leading edge of the spot, are presented in terms of disturbances relative to the unperturbed values in the laminar flow. Ensemble-averaged disturbances of U, V and T in the outer part of the spot are consistent with a picture of a relatively large vortical structure with a spanwise vorticity in the same sense as that of the laminar flow. A rather dominant feature of these distributions is the large negative disturbance in V and U near the leading edge in the outer part of the spot; associated with this disturbance is a positive perturbation in T. The terms contributing to the ensemble-averaged values of UV, UT and VT are obtained and discussed. In the case of UV, contributions by the disturbance are found to be of the same order as those by the random turbulence superposed on the disturbance. For VT, the disturbance appears to play a more dominant role in the transfer of heat. The conical property of the spot is tested for disturbance temperature and velocity fields by comparing contours, at three streamwise stations, of the velocity and temperature disturbances using the co-ordinates introduced by Cantwell, Coles & Dimotakis (1978). The results show that the conical transformation, which was found to be a good approximation for the full velocity field, is not an accurate representation for the disturbance fields of velocity and temperature measured relative to laminar values. An alternative viscous transformation represents more accurately the disturbance fields. Features of the turbulence within the spot are compared with those obtained in a fully turbulent boundary layer.

1. Introduction

The turbulent spot, first observed by Emmons (1951), has recently received a resurgence of interest reflected mainly in a number of relatively detailed experimental investigations (e.g. Wygnanski, Sokolov & Friedman 1976, hereafter referred to as I; Cantwell *et al.* 1978). The interest stems mainly from the notion, expressed by Wygnanski (1978), that a transitional spot is an orderly structure which may be considered as the basic module or building-block of a turbulent boundary layer. This interest becomes ever more compelling when one views other flows in a similar fashion. Indeed, the possibility of a close relationship between the slug (or puff) and the fully developed turbulent pipe flow and of a strong connection between the instability in a laminar mixing layer with the structure of a turbulent mixing layer has already been indicated by Wygnanski.

It seems appropriate to review briefly some of the arguments that have been put forward in favour of the spot as a basic structure of the turbulent boundary layer. Zilberman, Wygnanski & Kaplan (1977) (also Haritonidis, Kaplan & Wygnanski 1978) were able to educe the signature of an artificially produced spot (introduced in a laminar boundary layer prior to tripping) in a fully developed turbulent boundary layer. The survival of the spot over a relatively large distance (at least 100 boundary-layer thicknesses) in a turbulent environment is perhaps not too surprising in view of the well-established relatively long memory of the outer part of the boundary layer to disturbances introduced either at the wall or in the free stream. Perhaps more surprising is Zilberman *et al.*'s (1977) conclusion that reasonable agreement exists between the structure of the educed spot and the structure inferred for the large-eddy (or outer-layer bulge) structure from correlation measurements (e.g. Kovasznay, Kibens & Blackwelder 1970) in a turbulent boundary layer. Recently, Wygnanski, Haritonidis & Kaplan (1979) observed a pair of oblique wave packets following the passage of an isolated turbulent spot in a laminar boundary layer. These packets were identified as Tollmien–Schlichting waves whose subsequent breakdown produced new transitional spots. The possibility of a regeneration mechanism of the turbulent spot certainly would make the spot a plausible candidate for the basic module of a turbulent boundary layer even though the occurrence of a regeneration mechanism in a turbulent environment still needs to be established. It is interesting to note that Amini (1978, 1979) observed that contours, in a spanwise plan view, of the velocity perturbation associated with an incipient spot (artificially generated by a weak point disturbance) prior to formation of a turbulent spot are quite similar to the pattern observed by Zilberman *et al.* in a turbulent boundary layer. It should also be noted, however, that differences do exist between the large structure educed by Zilberman *et al.* and that associated with the turbulent spot in a laminar boundary layer. These differences, already noted by Zilberman *et al.*, would seem to preclude an interpretation of a turbulent boundary layer as a simple linear superposition of transitional spots. From a more pragmatic point of view, Coles & Barker (1975) were able to synthesize a turbulent boundary layer starting with a number of spots artificially created at several spanwise locations.

Van Atta & Helland (1980) explored the use of temperature as a passive tracer to provide some insight into the structure of a turbulent spot. Their temperature measurements within a turbulent spot that grew in a laminar boundary layer on a strongly

heated flat plate suggested a strong anticorrelation between temperature and longitudinal velocity disturbances, measured relative to the Pohlhausen and Blasius profiles respectively. No quantitative measure of the degree of correlation of these disturbances was obtained, as the strong heating (the difference ΔT between the wall temperature and free-stream temperature was 80 °C) precluded velocity measurements which would not be unduly affected by the temperature fluctuations. There has, to date, been no published estimate of the Reynolds shear stress within a spot or indeed of the contribution of the proposed coherent structure of the spot to this shear stress.† In this paper, simultaneous measurements of the longitudinal and lateral fluctuations and of the temperature fluctuation along the plane of symmetry of the spot in a slightly heated ($\Delta T \simeq 10$ °C) laminar boundary layer are used to quantify the contribution of the velocity and temperature disturbances, relative to the laminar values, to the momentum and heat transport within the spot. An attempt is also made to quantify the contribution to these fluxes from the turbulent fluctuations that are superposed on the disturbance. Simultaneous temperature traces obtained from a vertical rake of cold wires are examined and compared with those obtained in a turbulent boundary layer.

2. Experimental conditions

The basic experimental set-up used here is that described by Van Atta & Helland (1980). All measurements were made at a nominal free-stream velocity U_∞ of 11 m s^{-1} and a nominal value of 10 °C for ΔT. The sewing needles across which the spark was discharged protruded a height of about 1 mm into the boundary layer at a distance of 0·29 m from the leading edge of the plate. The centre of the gap between the needles was located on the centre-line ($z = 0$) of the working section. The frequency of the square wave used to trigger the spark discharge unit was 1·5 Hz, corresponding to a duration between discharges of 333 ms. Most of the measurements presented here were obtained at distance x_s (subscript s denotes the distance from the spark) of 0·54, 0·84, 1·06 and 1·12 m. Measurements were made both at $z = 0$ and at spanwise locations (for a given value of x_s) situated along rays emanating from the spark location ($x_s = 0$) at angles of $\pm 3{\cdot}5°$, $\pm 7°$ and $\pm 10{\cdot}5°$, measured relative to the x axis. The streamwise pressure gradient, measured with pressure tappings along the ceiling of the working section, was found to be small, though favourable, and in good agreement with the value calculated from free-stream acceleration measurements of

$$\frac{\delta^2}{\nu}\frac{dU_\infty}{dx} = 3{\cdot}1,$$

where δ is the laminar boundary-layer thickness at $U/U_\infty \simeq 0{\cdot}99$ and ν is the kinematic viscosity of air. No significant lateral pressure gradient or laminar base flow velocity variations could be detected at the measurement stations.

For U, V, T measurements, the instantaneous longitudinal velocity U and normal velocity V were measured with a miniature DISA X-wire (5 μm diameter Pt-coated

† Wygnanski (1978) briefly mentions that preliminary measurements with an X-wire are consistent with a momentum transport mechanism within the spot whereby a slowly rotating large eddy transports high-momentum fluid from the outer part of the boundary layer to the wall region.

tungsten wire approximately 2 mm long). A cold-wire (0·6 μm diameter Wollaston wire approximately 1 mm long) was placed next to the X-wire to measure the instantaneous temperature fluctuation T. To avoid errors due to radiation between prongs and wire as discussed by Fiedler (1979) only the central half of the silver coating of the Wollaston wire was etched.

At $x_s = 0{\cdot}54$ and 0·84 m, the cold wire was above (1·7 mm) and upstream (-2 mm) of the geometrical centre of the X-wire. At $x_s = 1{\cdot}12$ m, the cold wire was 0·3 mm above and approximately 1 mm upstream of the X-wire. A series of U–T measurements was also made at $x_s = 1{\cdot}06$ m with a two-wire probe having a single horizontal hot-wire and parallel cold-wire mounted 1 mm below the hot-wire. The hot-wires were operated by DISA 55M10 constant-temperature anemometers at an overheat of 0·6–0·8. The cold-wires (Pt–10 % Rh) were operated by constant-current anemometers with a current of 0·1 mA and a gain of 10^4. The frequency response of the cold-wire extended from d.c. to approximately 3 kHz (-3 dB point) at a speed of 8 m s^{-1}. Distances of both wires to the wall were determined to within 0·10 mm by viewing the wires and their reflections in the polished aluminium plate with a travelling telescope cathetometer.

For the present experimental conditions, parasitic velocity sensitivity of the 0·6 μm cold-wire and temperature sensitivity of the 5 μm hot-wires were negligibly small, except perhaps for the y position closest to the wall. Champagne (1979) has expressed the temperature sensitivity of a hot-wire in terms of the linearized voltage output obtained by direct calibration of the wire. Using Champagne's expression, the largest contribution of the temperature fluctuation to the measured ensemble mean and r.m.s. values (see § 3 for definitions) of the longitudinal velocity is estimated to be about 2·7 % at the measuring location nearest the wall, where the difference between local and free-stream temperatures is largest. No correction has been applied to the data for this estimated parasitic sensitivity. The X-wire was calibrated for both speed and yaw in the free stream at each x_s location before and after the y traverse at that particular location. For the yaw calibration, the X-wire was rotated in the x, y plane through the angles $\pm 2{\cdot}5°$, $\pm 5{\cdot}0°$ and $\pm 9{\cdot}0°$. The effective angles of the wires with respect to the flow were then determined by a method similar to that outlined in Bradshaw (1971, p. 123). Willmarth & Bogar (1977) observed much larger yaw angles using a miniature X-wire probe in close proximity to the surface. The angle estimated using $\tan^{-1}(V_l + \tilde{V} + 2|v'|)/(U_l + \tilde{U} - 2|u'|)$ from results given in figure 4 at $tU_\infty/x_s \simeq 1{\cdot}5$, see § 3 for definitions, is about 18° at the smallest y position considered here. As y increases this angle decreases, and the error in U and V due to large instantaneous yaw angles (outside the calibration range of $\pm 9°$) should be small everywhere except in the vicinity of the plate surface. The free-stream velocity was measured with a Pitot static tube connected to an MKS Baratron pressure transducer. Free-stream velocity U_∞ and temperature T_∞ were continuously monitored throughout the experiment.

Voltages from the hot and cold wires were recorded after being passed through buck and gain units on a 4-track FM tape recorder (Hewlett–Packard 3960A). The square-wave spark generator signal was also recorded. The signals were later played back at the same tape speed as recording (3·75 in. s^{-1} and digitized using a 12 bit, including sign, analog-to-digital converter) at a sampling frequency of 3200 Hz into a digital computer. We note that for ensemble-averaged measurements of the type considered here

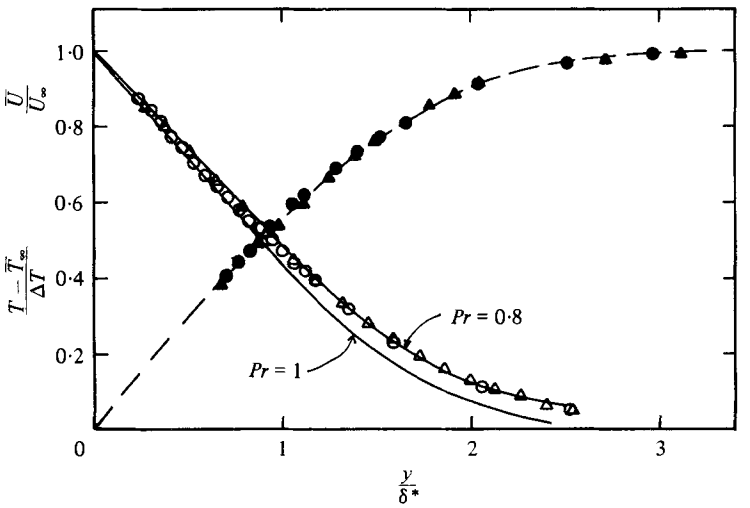

FIGURE 1. Velocity and temperature profiles in the laminar boundary layer. ○, x_s = 1·06 m; △, 0·74 m; solid symbols, $\bar{U}$; open symbols, $\bar{T}$; – – –, Blasius; ——, Pohlhausen.

consideration of a Nyquist sampling criterion and associated analogue filtering is not required.

A vertical array of four cold-wires (0·6 μm diameter, 1 mm length) was used for simultaneous visual examination of the behaviour of temperature signals at several levels within a turbulent spot. These four signals together with a signal from a hot-wire located next to one of the cold-wires and the square-wave signal were recorded on an 8-track FM tape recorder (Hewlett–Packard 3968A). The tape was later played back at a different speed into a multi-channel strip chart recorder for display of simultaneous traces.

Mean velocity and mean temperature profiles measured with no spark but with spark needles left in position were found to be in good agreement with the Blasius and Pohlhausen profiles respectively, as shown in figure 1. The slope of the experimental temperature profile at the wall is slightly lower than the prediction of Pohlhausen, given by (e.g. Schlichting 1968)

$$\frac{\delta^*}{\Delta T}\frac{\partial(\bar{T}-T_\infty)}{\partial y} = 0{\cdot}5713Pr^{\frac{1}{3}} \quad (0{\cdot}6 < Pr < 10),$$

where Pr is the molecular Prandtl number and δ^* is a displacement thickness. For $Pr = 0{\cdot}8$, the above relation yields a slope of magnitude equal to 0·53, while our estimates for the experimental values are 0·56 and 0·54 at $x_s = 1{\cdot}06$ and 0·74 m respectively.

3. Definition of ensemble averages

Ensemble averages of the instantaneous signals U, V and T were obtained by first determining the position of the leading edge (L.E.) of the spot. The ensemble-averaging operation was performed after individual realizations of U, V and T had been aligned with respect to the L.E. A quantitative comparison between averaging relative to the spark and averaging relative to the L.E. by Van Atta & Helland (1980) showed that

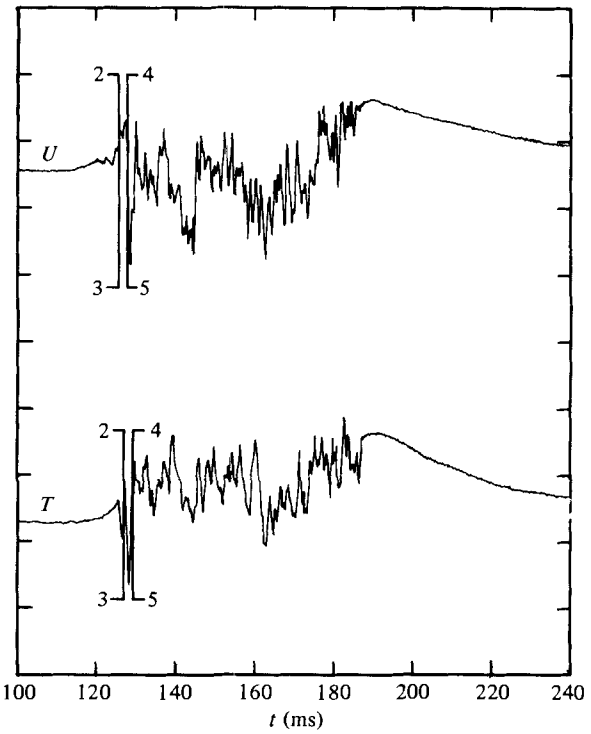

FIGURE 2. Typical velocity (upper) and temperature traces with leading-edge positions indicated for various values of k. (Scale for ordinate is arbitrary.) $x_s = 1{\cdot}06$ m; $y/h = 0{\cdot}09$.

leading-edge averaging sharpens the mean gradients, as expected, but has no discernible effect on the ensemble-averaged fluctuations.

The L.E. of the spot was found by applying the following criterion

$$\left|\frac{\partial X}{\partial t}\right| > k\left|\frac{\partial X}{\partial t}\right|_{\max},$$

where X stands for U or T and the subscript max refers to the maximum value of the time derivative well in advance of arrival of the spot. This value was determined after examining computer-plotted traces of U and T for a number of realizations. The absolute values in the inequality were required because X can either initially increase or decrease, relative to its laminar value, at the L.E. of the spot. The magnitude of k, which was ultimately kept constant, equal to 3, for all values of y considered here, was initially obtained by trial and error by examining the position of the L.E. on many traces of U and T.

It is clear from figure 2 that the result is insensitive to the actual value of k because of the relatively sharp change in U and T near the L.E. of the spot. The final choice of $k = 3$ was a compromise as too large a value of k would, for most realizations, erroneously delay the determination of the L.E. while too small a value of k could cause this edge to be sometimes chosen well ahead of the actual start of the spot. Almost every realization that was examined visually indicated that L.E. locations corresponding to $k = 3$ were identical to those corresponding to $k = 2$. For many realizations, $k = 4$ and $k = 3$ also yielded identical L.E. locations.

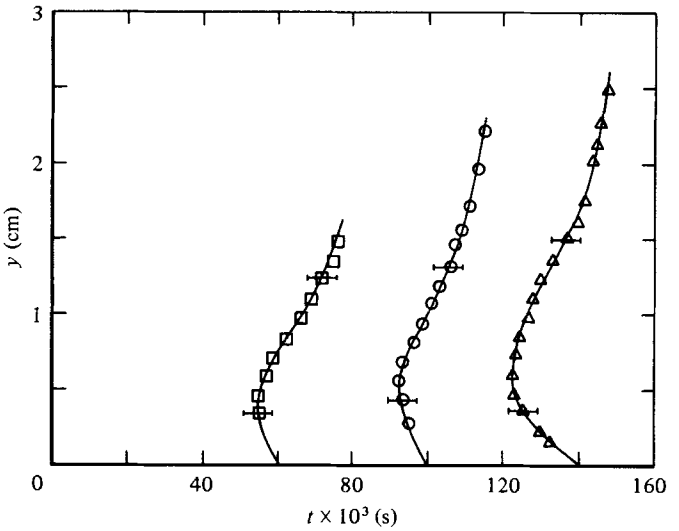

FIGURE 3. Arrival time of leading edge at different distances from the surface. □, station 1; ○, station 2; △, station 3. Horizontal bar indicates standard deviation.

After choosing the L.E. of a realization, 384 sequential samples, from a total of 720, were retained and preserved on a permanent basis on digital magnetic tape. The first 60 samples were ahead of the L.E. and 384 samples were used in the final data processing to reduce computing time with no loss of information, since the spot was always situated well within the selected sampling range. Values of U, V and T were averaged, over an ensemble of typically 200 realizations, after alignment relative to the L.E. The leading edge of V was assumed to be identical to that of U. When considering ensemble averages of the product UT (or VT), the effective L.E. was assumed to be given by the arithmetic mean of L.E. positions for U and T. A few realizations were rejected because the L.E. was found to occur at either a very small or very large duration, as measured from the firing of the spark. For the present experiment a rather relaxed criterion was used in the rejection procedure as the lower and upper bounds on duration were set at approximately 34 and 200 ms respectively. The maximum rejection rate for records of U (or V or UV), T and UT (or VT) did not exceed 2 %. The location of the L.E., based on the temperature criterion, is shown in figure 3 as a function of x_s and y, the distance from the plate. The height of the overhang, which corresponds to the earliest arrival of the L.E. at a particular x_s, increases slightly with x_s. The standard deviation of the L.E., shown by horizontal bars in figure 2, does not vary significantly with y and while it increases, as expected, with x_s its magnitude remains small (typically about 5 % of the L.E. value).

Instantaneous velocity and temperatures can be decomposed as follows

$$U = U_l + \tilde{U} + u, \tag{1}$$

$$V = V_l + \tilde{V} + v, \tag{2}$$

$$T = T_l + \tilde{T} + \theta, \tag{3}$$

where the subscript l refers to the value in laminar flow and $\tilde{U}$, $\tilde{V}$ and $\tilde{T}$ are the ensemble-averaged values of $U - U_l$, $V - V_l$, $T - T_l$ respectively, i.e. with angular

brackets denoting ensemble averages, $\tilde{U}$, $\tilde{V}$, $\tilde{T}$ are given by

$$\tilde{U} = \langle U \rangle - U_l, \tag{4}$$

$$\tilde{V} = \langle V \rangle - V_l, \tag{5}$$

$$\tilde{T} = \langle T \rangle - T_l, \tag{6}$$

and represent the ensemble-averaged disturbances, relative to the undisturbed laminar flow, produced by the spots. A decomposition, similar to that given by equations (1)–(3), was used by Hussain & Reynolds (1970) to describe the mechanics of an organized wave in a turbulent flow. In their case, however, the angular brackets denote a phase average while X_l is replaced by the conventional time average $\bar{X}$. It follows from equations (1)–(3) that

$$\langle u \rangle = \langle v \rangle = \langle \theta \rangle = 0.$$

The ensemble-averaged values of the products UV, UT and VT are given by

$$\langle UV \rangle = \langle U \rangle \langle V \rangle + \langle uv \rangle, \tag{7}$$

$$\langle UT \rangle = \langle U \rangle \langle T \rangle + \langle u\theta \rangle, \tag{8}$$

$$\langle VT \rangle = \langle V \rangle \langle T \rangle + \langle v\theta \rangle, \tag{9}$$

as the organized motion and the background turbulence are, on average, uncorrelated. The r.m.s. values of the fluctuations, defined in an ensemble sense, are denoted by

$$u' = \langle (U - \langle U \rangle)^2 \rangle^{\frac{1}{2}} = \langle u^2 \rangle^{\frac{1}{2}}, \tag{10}$$

$$v' = \langle (V - \langle V \rangle)^2 \rangle^{\frac{1}{2}} = \langle v^2 \rangle^{\frac{1}{2}}, \tag{11}$$

$$\theta' = \langle (T - \langle T \rangle)^2 \rangle^{\frac{1}{2}} = \langle \theta^2 \rangle^{\frac{1}{2}}. \tag{12}$$

4. Ensemble-averaged velocity and temperature results

Distributions of $\tilde{U}/U_\infty$, $\tilde{V}/U_\infty$, $\tilde{T}/\Delta T$ at $x_s = 0{\cdot}84$ m (station 2) for different values of y are shown in figures 4(a, b, c) as a function of time t, measured from the firing of the spark. For the purpose of presentation and to facilitate discussion and comparison with results of I, t is normalized by U_∞ and x_s while y is normalized by the height of the spot h. The difficulty of precisely determining h has already been discussed in I. For our present purpose, h was taken, somewhat arbitrarily, to be the maximum height ($= 2{\cdot}25$ cm) of the 1 % contour of $\tilde{T}/\Delta T$. Although there will be inevitable jitter in the height of each individual spot, it is worth pointing out that a determination of the average height on the basis of the temperature disturbance is more likely to be accurate than one based on the velocity disturbance since the potential flow disturbance associated with the spot is present at distances much greater than h. As shown in figure 4, the L.E. location for $\tilde{U}$ (or $\tilde{V}$) is slightly different from that of $\tilde{T}$ as a result of the small displacement of the temperature and X-wires. The differing values of y/h for velocity and temperature results are a consequence of this displacement.

FIGURE 4. Ensemble-averaged velocity and temperature profiles at station 2 ($x_s = 0{\cdot}84$ m). (a) $\tilde{U}/U_\infty$; (b) $\tilde{V}/U_\infty$; (c) $\tilde{T}/\Delta T$; (d) $(u' - u'_l)/U_\infty$; (e) $(v' - v'_l)/U_\infty$; (f) $(\theta' - \theta'_l)/\Delta T$; ($g$) $\langle uv \rangle / U_\infty^2$; ($h$) $\langle u\theta \rangle / U_\infty \Delta T$; ($i$) $\langle v\theta \rangle / U_\infty \Delta T$.

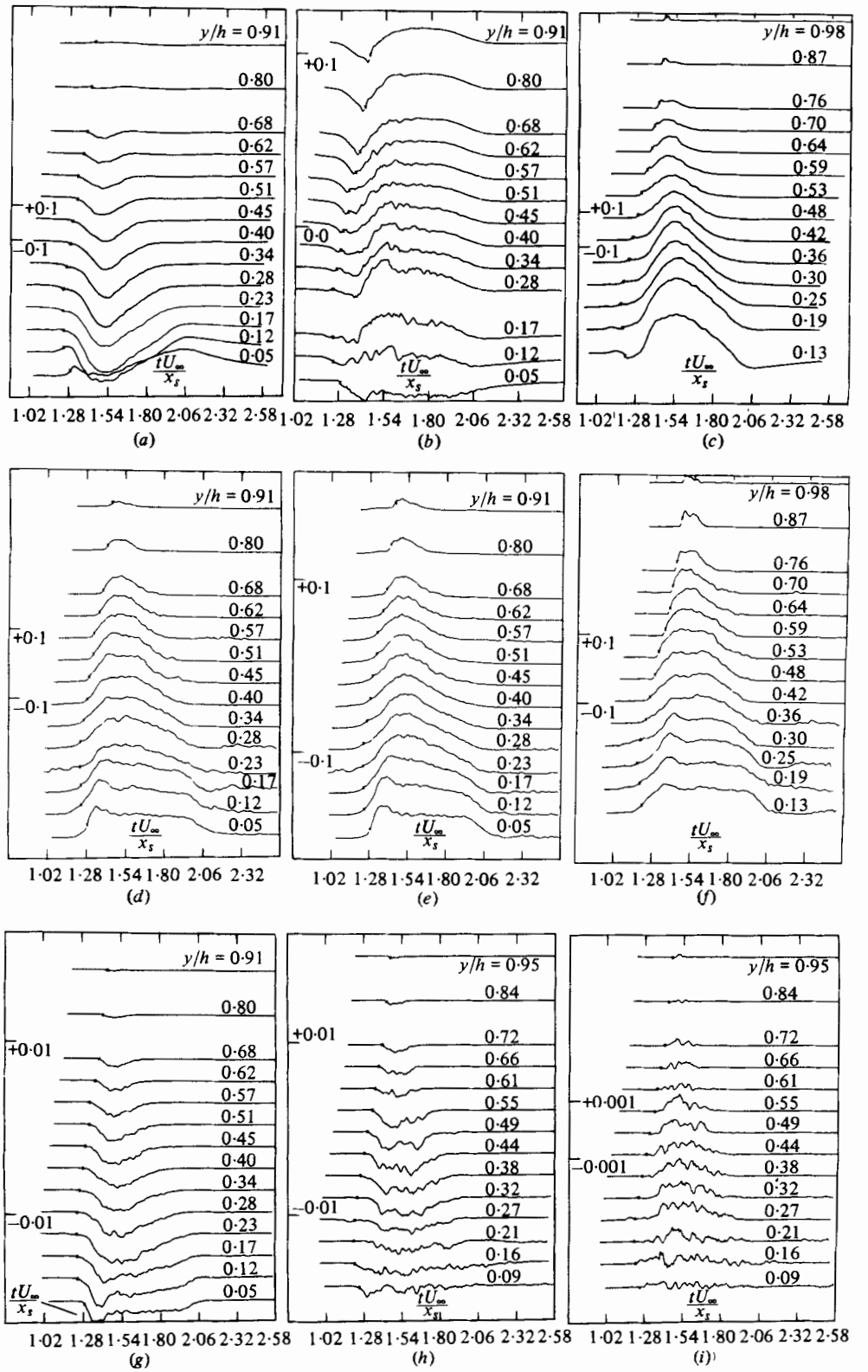
y/h = 0·91
0·80
0·68
0·62
0·57
0·51
+0·1
0·45
0·40
−0·1
0·34
0·28
0·23
0·17
0·12
0·05
tU∞/xs
1·02 1·28 1·54 1·80 2·06 2·32 2·58
(a)
y/h = 0·91
+0·1
0·80
0·68
0·62
0·57
0·51
0·45
0·0
0·40
0·34
0·28
0·17
0·12
0·05
tU∞/xs
1·02 1·28 1·54 1·80 2·06 2·32 2·58
(b)
y/h = 0·98
0·87
0·76
0·70
0·64
0·59
0·53
+0·1
0·48
0·42
−0·1
0·36
0·30
0·25
0·19
0·13
tU∞/xs
1·02 1·28 1·54 1·80 2·06 2·32 2·58
(c)
y/h = 0·91
0·80
0·68
0·62
+0·1
0·57
0·51
0·45
0·40
−0·1
0·34
0·28
0·23
0·17
0·12
0·05
tU∞/xs
1·02 1·28 1·54 1·80 2·06 2·32
(d)
y/h = 0·91
0·80
+0·1
0·68
0·62
0·57
0·51
0·45
0·40
0·34
0·28
−0·1
0·23
0·17
0·12
0·05
tU∞/xs
1·02 1·28 1·54 1·80 2·06 2·32
(e)
y/h = 0·98
0·87
0·76
0·70
0·64
0·59
+0·1
0·53
0·48
0·42
−0·1
0·36
0·30
0·25
0·19
0·13
tU∞/xs
1·02 1·28 1·54 1·80 2·06 2·32
(f)
y/h = 0·91
0·80
+0·01
0·68
0·62
0·57
0·51
0·45
0·40
0·34
0·28
−0·01
0·23
0·17
0·12
0·05
tU∞/xs
1·02 1·28 1·54 1·80 2·06 2·32 2·58
(g)
y/h = 0·95
0·84
+0·01
0·72
0·66
0·61
0·55
0·49
0·44
0·38
0·32
−0·01
0·27
0·21
0·16
0·09
tU∞/xs
1·02 1·28 1·54 1·80 2·06 2·32 2·58
(h)
y/h = 0·95
0·84
0·72
0·66
0·61
+0·001
0·55
0·49
0·44
−0·001
0·38
0·32
0·27
0·21
0·16
0·09
tU∞/xs
1·02 1·28 1·54 1·80 2·06 2·32 2·58
(i)

The $\tilde{U}$ and $\tilde{T}$ distributions obtained with the X-wire/cold-wire combination agreed well with those obtained with the single hot-wire/cold-wire combination. Near the wall ($y/h < 0{\cdot}12$), there is a sudden acceleration at the L.E. of the spot followed by an equally sudden deceleration prior to a slow increase in $\tilde{U}$ as the trailing edge (T.E.) is neared. A maximum value of $\tilde{U}$ is recorded near the T.E., beyond which velocity fluctuations cease to exist. Beyond this maximum, there is a slow recovery back to the laminar value that existed ahead of the spot. For $y/h < 0{\cdot}12$, the temperature disturbance $\tilde{T}$ (not shown), as obtained from the parallel wire combination at $x_s = 1{\cdot}06$ m, exhibits a sudden decrease followed by an increase (these changes are sharper than those of $\tilde{U}$) near the L.E. There is a slow decrease in temperature towards the T.E. with the minimum value in $\tilde{T}$ occurring at approximately the position where $\tilde{U}$ is maximum. Downstream of the T.E., the temperature relaxes, in a roughly exponential fashion, back up to the value corresponding to the undisturbed laminar flow upstream of the spot. The relaxation of the temperature downstream of the disturbance appears to be somewhat faster than that of $\tilde{U}$. The increase in the wall shear stress, or skin friction coefficient, towards the T.E. edge of the spot has been noted in I. The behaviour of $\tilde{U}$ close to the wall supports this observation while the behaviour of $\tilde{T}$ clearly suggests an increase in the wall heat flux towards the T.E.

For $y/h > 0{\cdot}12$, $\tilde{U}$ is negative (figure 4*a*) throughout the spot, exhibiting a decrease followed by a somewhat slower increase towards the T.E. $\tilde{T}$ is positive (figure 4*c*) throughout the spot but exhibits the same slight asymmetry as $\tilde{U}$. Positions corresponding to a minimum $\tilde{U}$ or maximum $\tilde{T}$ do not change significantly with y. For $0{\cdot}24 < y/h < 0{\cdot}44$, the recovery of both $\tilde{U}$ and $\tilde{T}$ after the T.E. of the spot has passed the wires appears to be almost immediate. The small bump appearing on both $\tilde{U}$ and $\tilde{T}$ at the position of the L.E. is probably a result of the alignment procedure described earlier. This bump is present in the data of I where a sudden dip near the trailing interface of the spot was also noted. The dip was interpreted as representing the signature of a small coherent eddy near the interface of the spot.

For $y/h > 0{\cdot}4$, the induced velocity field of the spot is reflected in the behaviour of $\tilde{U}$ behind the T.E. $\tilde{U}$ exhibits a definite dip (the scale in figure 4 is too small to observe this dip clearly) in this region of the flow prior to a slow increase towards the laminar value. At larger values of y, a dip may be observed ahead of the L.E. prior to an increase in $\tilde{U}$ as the L.E. is approached. The velocity perturbation associated with the induced flow field of the spot has been observed to a distance of about 15 spot heights or 30 laminar boundary-layer thicknesses from the plate. The potential flow signature has a roughly sinusoidal form at these large values of y. Outside the spot there is, not surprisingly, no detectable temperature perturbation.

Distributions of $\tilde{V}$ are shown in figure 4(*b*) (note that the scale for $\tilde{V}$ is one order of magnitude larger than that for $\tilde{U}$). At $y/h = 0{\cdot}05$, $\tilde{V}$ is negative throughout the spot, which suggests that the cooler region close to the wall is associated with fluid which is swept to the wall from a higher level in the boundary layer and arrives with a streamwise velocity excess. The minimum value of $\tilde{V}$ occurs approximately where the local streamwise acceleration has nearly vanished. At larger t, $\tilde{V}$ exhibits a plateau ($\partial\tilde{U}/\partial t$ is positive over this region) and does not show a local minimum near the T.E. of the spot where $\tilde{U}$ is maximum. In the relaxation region upstream of the spot, $\tilde{V}$ slowly increases to its undisturbed laminar value. As y increases, the decrease in $\tilde{V}$ near the L.E. is followed by a relatively sharper increase with a maximum occurring

roughly where $\tilde{U}$ is minimum (or $\tilde{T}$ is maximum). For y/h greater than about 0·4, $\tilde{V}$ is negative at or very near the L.E. before exhibiting a conspicuous increase towards positive values in the central and T.E. regions of the spot. This feature is in good qualitative agreement with the observation in I that the component of velocity normal to the surface is directed towards the plate near the leading interface and away from it in the remaining part of the spot. It is clear from figure 4(*b*) that the magnitude of the minimum in $\tilde{V}$ near the L.E. increases with increasing y while the maximum (positive) $\tilde{V}$ decreases in magnitude as y increases.† This trend is also noted at the other two stations. The negative $\tilde{V}$ near the L.E. also appears in the potential flow disturbance above the spot, as does the positive plateau of $\tilde{V}$ that extends well beyond the T.E. (a rough indication of the T.E. location may be obtained by reference to the $\tilde{T}$ distributions in figure 4*c*). It should be noted that the potential flow signature would be clearly visible in the $\tilde{U}$ distributions if the vertical scale in figure 4(*a*) were suitably expanded. It is worth comparing the $\tilde{V}$ distribution at $y/h = 0{\cdot}51$ (or 0·57) with that reported in I at $y/h = 0{\cdot}54$ (their figure 23). Although the nearly constant value of $\tilde{V}/U_\infty$ ($\simeq 0{\cdot}01$) on the plateau (that extends both upstream and downstream of the T.E.) is in very good agreement with the value in I, the present minimum in V at the L.E. is only $-0{\cdot}01U_\infty$,‡ as compared with about $-0{\cdot}03U_\infty$ in I. Part of this discrepancy may be due to the relatively low accuracy of the V measurements, as was pointed out in I. Differences in the method used to form the ensemble averages might also contribute. While the present $\tilde{V}$ is based on a L.E. average, the distributions in I are generally based on a combination of L.E. and T.E. averages. In I the sharply positive fluctuation (of order $0{\cdot}01U_\infty$) in $\tilde{V}$ that was recorded near the T.E. disappeared completely when $\tilde{V}$ was L.E. averaged. Since $\tilde{V}$ obtained by T.E. averaging alone was not presented, it is not clear what fraction of $\tilde{V}$ at or near the L.E. is associated with their L.E. averaging. The $\tilde{V}$ distribution using the continuity equation

$$\partial\tilde{U}/\partial x + \partial\tilde{V}/\partial y = 0$$

and assuming that $\partial\tilde{W}/\partial z$ is zero in the plane of symmetry of the spot was also calculated and, while the calculation was in good agreement with the measurements, a note of caution is required in view of the assumptions involved in the calculation (e.g. Taylor's hypothesis to convert $\partial\tilde{U}/\partial t$ into $\partial\tilde{U}/\partial x$). Also the direct measurements reported in I indicated that $\tilde{W}$ and $\partial\tilde{W}/\partial z$ were small but perhaps not negligible at $z = 0$.

Distributions of r.m.s. velocities u', v', and r.m.s. temperature θ' are shown in figures 4(*d*, *e*, *f*). For the purpose of presentation only, these distributions have been plotted (all curves in figure 4 were plotted by computer) after subtraction of the r.m.s. velocity and temperature§ in the laminar flow. Values of u'_l, v'_l, θ'_l are in fact conditional averages obtained in the laminar region at much earlier times (over the region 5–40 samples; the L.E. occurs at the 60th sample) than the L.E. of the spot. The distributions of u', v', θ' exhibit a number of common characteristics at small values of y. In particular, there is a significant peak in all three quantities near the

† For y/h greater than unity, both maximum and minimum values of $\tilde{V}$ would again decrease due to the decay of the potential flow disturbance with distance from the ridge of the spot.

‡ V_l is several orders of magnitude smaller.

§ Ideally, these laminar quantities should be zero. The present non-zero but small values of u'_l or v'_l are associated with very low-frequency irrotational fluctuations, while θ'_l is mainly due to electronic noise.

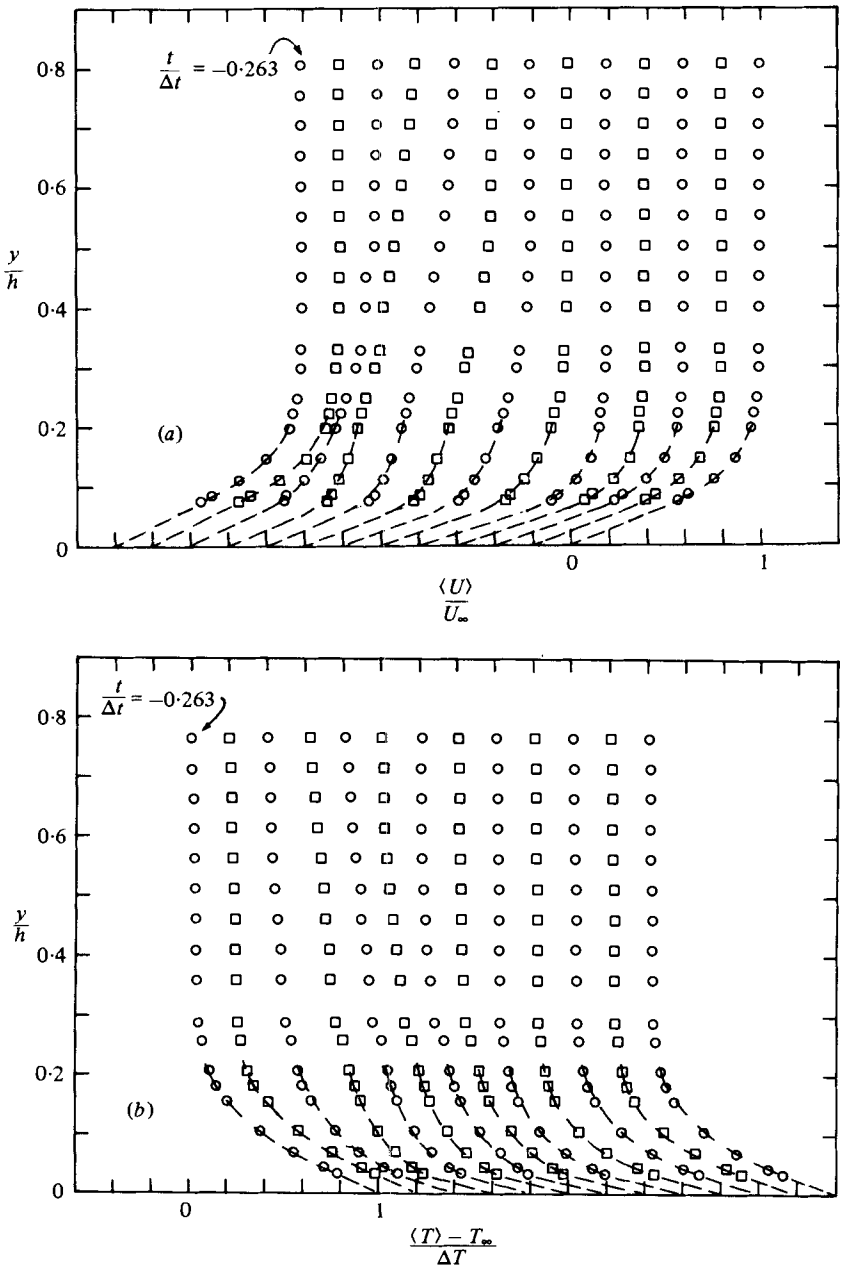

FIGURE 5. Ensemble-averaged velocity and temperature profiles at several positions through the spot at $x_s = 1{\cdot}06$ m. $-0{\cdot}263 \leqslant t/\Delta t \leqslant 1{\cdot}316$ in steps of 0·132. $\Delta t = 76$ ms. (*a*) Velocity. (*b*) Temperature.

L.E. followed by a plateau. This trend is the same as that reported for θ' by Van Atta & Helland (1980). There is also a sharp rise, especially in v' and u', very near the wall. As y increases, this increase is more gradual. Note also that, with increasing y, the peak and plateau first disappear in the u' and v' distributions but are still identifiable in θ'. At large y, u' and v' are roughly symmetrical with respect to the location of the ridge but θ' exhibits a sharp increase near the L.E. This is not surprising since we

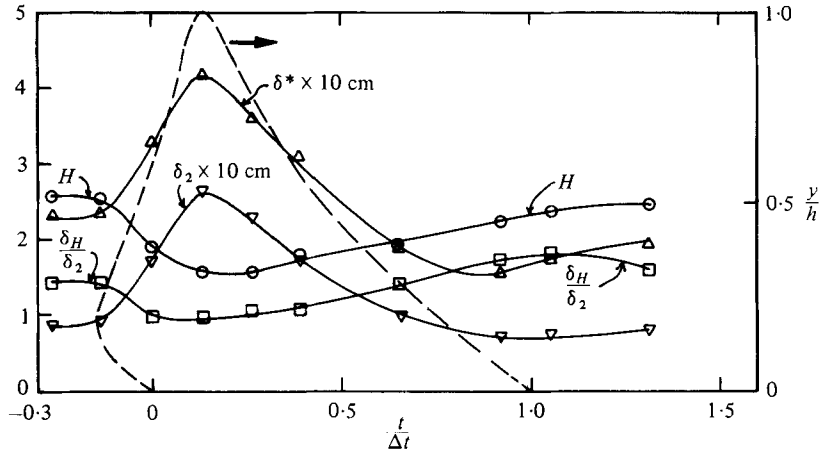

FIGURE 6. Variation of boundary-layer parameters through the spot at $x_s = 1{\cdot}06$ m.

expect the temperature jump across the thermal or vorticity interface to be much sharper than any corresponding velocity change. There is similar evidence of this in the outer part of slightly heated turbulent shear flows (e.g. Sreenivasan, Antonia & Britz 1979).

Distributions (figures 4*g*, *h*, *i*) of $\langle uv \rangle$, $\langle u\theta \rangle$ and $\langle v\theta \rangle$, again taken relative to the appropriate laminar zone averages, show that $\langle uv \rangle$ (figure 4*g*) is generally better behaved and less ragged than $\langle v\theta \rangle$ or $\langle u\theta \rangle$. The increased raggedness in the heat flux distributions is unlikely to be due to the separation between velocity and temperature wires; results for station 3, where the separation was much smaller, show a similar degree of raggedness. It is worth drawing attention to the large values of $\langle uv \rangle$ close to the wall near the L.E. and the absence of a maximum in $\langle uv \rangle$ towards the T.E. where the average wall shear stress is maximum. It is also worth pointing out that the locations where $\langle uv \rangle$, $\langle u\theta \rangle$, $\langle v\theta \rangle$ start to deviate from their undisturbed flow values correspond very approximately with the L.E. location.

Mean velocity and temperature profiles – deduced from ensemble-averaged data for U and T – are shown in figure 5 for various values of $t/\Delta t$, where Δt is the time taken for the spot to travel past the measurement station at the wall. The boundary-layer parameters δ^*, δ_2, H and the enthalpy thickness, defined as

$$\delta_H = \int_0^\infty (\langle U \rangle / U_\infty)[(\langle T \rangle - T_\infty)/\Delta T]\, dy,$$

were calculated from these data and are shown in figure 6. As in the data of I, the displacement thickness δ^* increases rapidly downstream of the L.E. overhang, reaches a maximum at a position where the height of the spot is maximum, and finally decreases towards the T.E. The momentum thickness δ_2 exhibits the same qualitative trend as the displacement thickness and, like δ^*, qualitatively follows the shape of the spot over a significant portion of its total duration. The shape parameter H and the ratio δ_H/δ_2 decrease suddenly near the tip of the overhanging L.E. before becoming approximately constant in the region where the height of the spot is maximum. In this region $H \simeq 1{\cdot}57$, which is only slightly larger than the value in I, while the momentum and enthalpy thicknesses are nearly equal. Although the value of H at

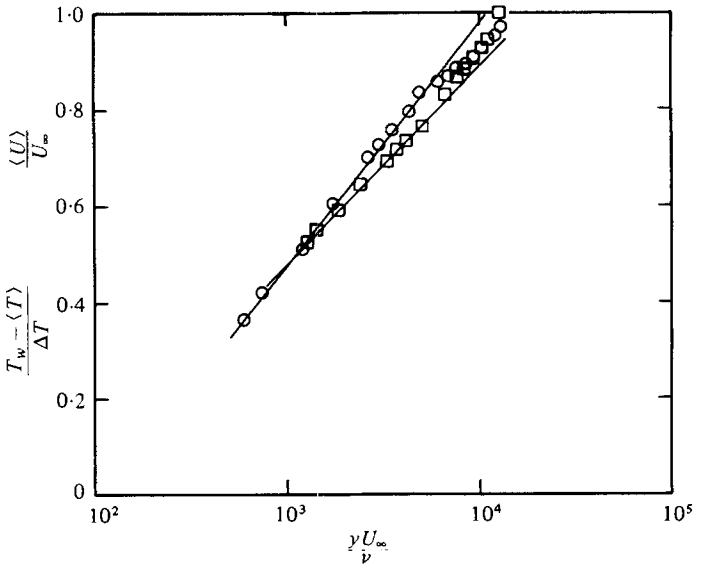

FIGURE 7. Semi-logarithmic velocity and temperature profiles for $t/\Delta t = 0{\cdot}13$ at $x_s = 1{\cdot}06$ m.

the T.E. is below that at the L.E., the ratio δ_H/δ_2 is larger at the T.E. than at the L.E. Note that at the tip of the L.E. (the spot in figure 6 is deduced from the 1 % θ' contour) $H \simeq 2{\cdot}6$, the Blasius value, whereas in I it was found that $H \simeq 1{\cdot}7$ and attributed this low value to the presence of fluctuations in the flow upstream of the spot. It should also be noted that values of δ^*, δ_2 and δ_H upstream of the L.E. tip were found to be in excellent agreement with values obtained in the laminar boundary layer and also with values corresponding to velocity and temperature profiles that were conditionally averaged in the laminar portion of the flow between the spark and the L.E. of the spot.

The velocity and temperature profiles at $t/\Delta t = 0{\cdot}13$ (which corresponds to the minimum position for H) have been re-plotted in figure 7 in semi-logarithmic coordinates. Although both profiles exhibit a linear region, it is clear that this region does not correspond to the universal log-law, apparently found in I and by Cantwell *et al.* (1978). As we do not have a reliable estimate of the wall shear stress τ_w, no attempt was made to plot the profiles using wall variables U_τ (friction velocity) and T_τ (friction temperature). If it is assumed that the slopes of the lines shown in figure 7 correspond to the slopes in the universal profiles

$$\frac{\overline{U}}{U_\tau} = \frac{1}{\kappa}\ln\frac{yU_\tau}{\nu} + C, \quad \frac{T_w - \overline{T}}{T_\tau} = \frac{1}{\kappa_\theta}\ln\frac{yU_\tau}{\nu} + C_\theta,$$

with $\kappa = 0{\cdot}41$ and $\kappa_\theta \simeq 0{\cdot}37$, unreasonably high values are obtained for the skin friction coefficient c_f ($= 0{\cdot}0108$) and the Stanton number ($= 1{\cdot}11c_f/2$). The resulting values of C ($= -4$) and C_θ ($\simeq -5{\cdot}8$) are clearly at variance with those generally accepted for a turbulent boundary layer with zero pressure gradient conditions. The Reynolds number R_{δ_2}, based on δ_2, for the present profiles is only 1787, but it is unlikely that this low value is responsible for the breakdown in the universal logarithmic profile. In any event, the value of R_{δ_2} in I, when $t/\Delta t$ corresponds to the

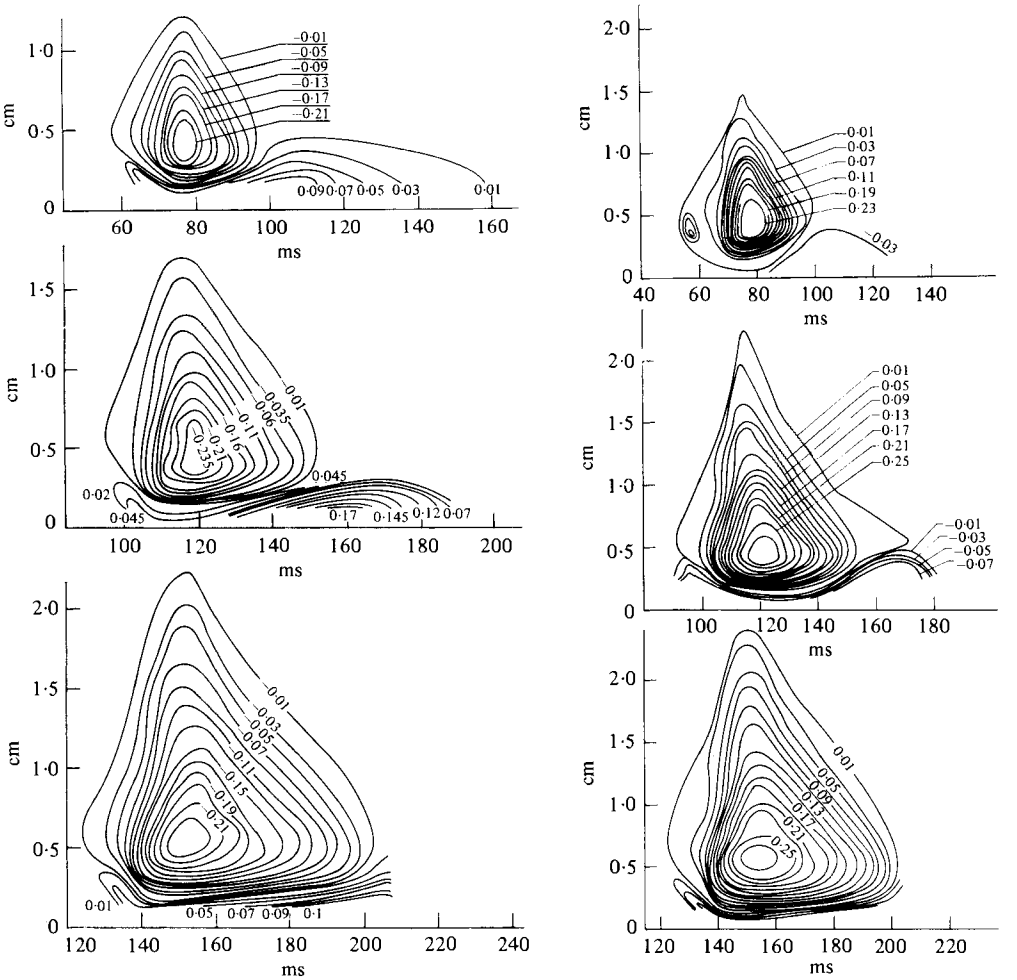

FIGURE 8. Isovelocity and isotemperature contours at the three stations (top and bottom correspond to stations 1 and 3 respectively). (*a*) Contours of constant $\tilde{U}/U_\infty$; (*b*) Contours of constant $\tilde{T}/\Delta T$.

maximum height of the spot, is only about 1500. Although the values of c_f obtained (presumably by extrapolation of U to the wall) in I appear reasonable ($c_f \simeq 5{\cdot}3 \times 10^{-3}$ near the T.E. as compared with $3{\cdot}6 \times 10^{-3}$ at the maximum spot height), there are too few experimental points (a criticism which can also be made of the present data) to categorically ascertain the existence of the universal log-law. Figure 20 of I suggests that, for the profile closest to the T.E., the log-region may extend to a value of y as large as $0{\cdot}33h$, whereas the spot itself extends only to $0{\cdot}25h$. Although the present velocity profile exhibits a wake component, as reported by Cantwell *et al.*, the temperature profile indicates a wake component that is negative, at least with respect to the chosen temperature log-law.

Contours of $\tilde{U}/U_\infty$ and $\tilde{T}/\Delta T$ at the three X-wire stations are shown in figures 8(*a*) and (*b*) respectively. Some of the salient features are:

(i) an outer region of velocity defect and temperature excess;

(ii) a region of cooler but higher-velocity fluid very near the wall. This region extends downstream of the L.E. associated with the outer structure and, particularly at station 1, well upstream of the T.E. of the outer structure (as indicated, for example, by the latest arrival of the $+1$ % contour of $\tilde{U}/U_\infty$);

(iii) close similarity in shape between $\tilde{U}$ and $\tilde{T}$, especially at stations 2 and 3. At station 1, the smaller set of temperature excess contours that occurs near the leading-edge overhang is not observed in the $\tilde{U}$ contours.

5. Results in conical co-ordinates

It was noted first in I that sufficiently far downstream from the disturbance all spot characteristics are independent of the type of disturbance. Cantwell *et al.* established the conical property for their ensemble-averaged velocity data at two out of three stations on a plate inserted in a low-speed water channel. They used a similarity transformation based on the property of conical growth to calculate instantaneous mean streamlines and to obtain mean particle paths in Galilean-invariant form, and introduced the similarity co-ordinates

$$\xi = \frac{x_s - x_0}{U_\infty(t - t_0)}, \quad \eta = \frac{y}{U_\infty(t - t_0)}$$

(x_0, t_0 are the virtual-origin co-ordinates) to describe the flow in the plane of symmetry of the spot. Presumably another co-ordinate $z/U_\infty(t - t_0)$ would be required to complete the three-dimensional description of the spot.

Cantwell *et al.* determined the virtual origin by geometrically constructing loci of certain features of their ensemble-averaged velocity traces at three stations. These features were chosen somewhat arbitrarily (e.g. location of first occurrence of a detectable change in velocity or location of the main velocity minimum). To determine x_0 and t_0 we chose to use the arrival times at the three stations of certain features associated with the measured contours of a number of different quantities. The majority of the data was provided by the locations of the earliest and latest arrivals of negative and positive contours of $\tilde{U}/U_\infty$ and $\tilde{T}/\Delta T$ respectively, of u'/U_∞ and $\langle uv \rangle / U_\infty^2$. One per cent contours were used except for $\langle uv \rangle / U_\infty^2$, where 0·05 % contours were used. Locations of the earliest and latest arrival times are shown in figure 9(*a*). Maximum heights of different $\tilde{T}/\Delta T$ contours are plotted against x_s in figure 9(*b*). Straight-line fits to these data suggest that reasonable choices for t_0 and x_0 (measured relative to the position of the spark) are -20 ms and -10 cm respectively. These values indicate that the virtual origin is located downstream ($x = 19$ cm) of the L.E. of the plate. Loci of maximum heights of different $\tilde{U}/U_\infty$ contours are consistent with these values of t_0 and x_0. Data (not shown here) based on $\tilde{T}/\Delta T = 0{\cdot}01$ at stations off the plane of symmetry† located along $\pm 3{\cdot}5°$ rays emanating from the disturbance also support ($t_0 = -20$ ms, $x_0 = -10$ cm) as a possible choice of co-ordinates for the virtual origin. It should be mentioned that other straight-line fits to the data in figure 9(*a*) would have yielded other solutions for x_0, t_0 (for example, a likely solution

† Cantwell *et al.* did not take measurements off the plane of symmetry but noted that the virtual origin for z, as judged from the observed rate of growth of motion picture records, could be closer to the disturbance source than the origin determined from their measurements in the (x, y) plane.

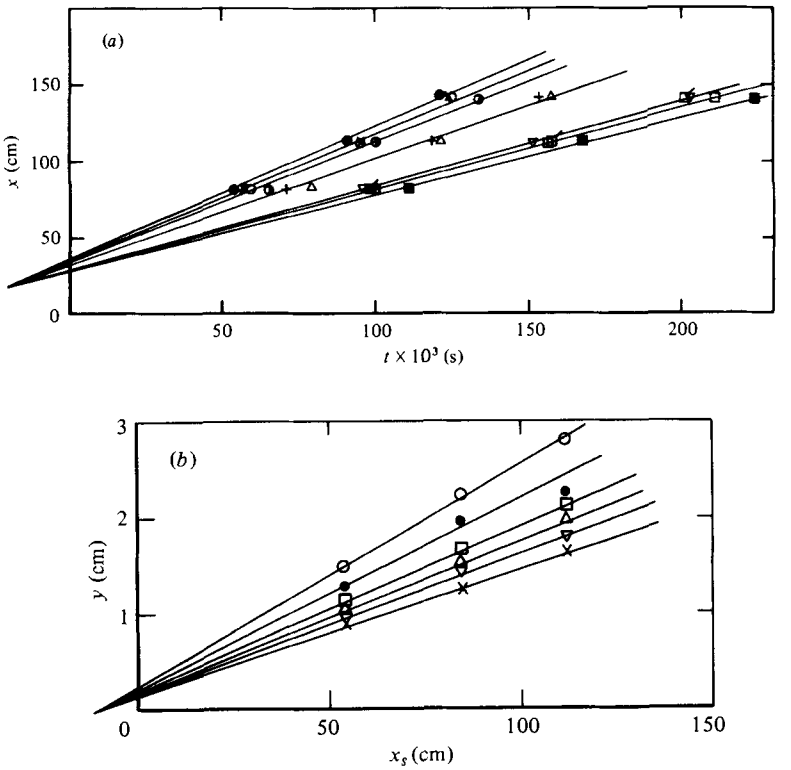

FIGURE 9. (*a*) Determination of x_0 and t_0 from arrival times of leading and trailing edges, based on velocity and temperature information in the plane of symmetry. ●, L.E., $\tilde{T}/\Delta T = 0{\cdot}01$; ■, T.E., $\tilde{T}/\Delta T = 0{\cdot}01$; △, maximum $\tilde{T}/\Delta T$; ×, L.E., $\tilde{U}/U_\infty = 0{\cdot}01$; ▽, T.E., $\tilde{U}/U_\infty = 0{\cdot}01$; +, minimum $\tilde{U}/U_\infty$; ○, L.E., $u'/U_\infty = 0{\cdot}01$; □, T.E., $u'/U_\infty = 0{\cdot}01$; ◑, L.E., $\langle uv\rangle/U_\infty^2 = 0{\cdot}0005$; □, T.E., $\langle uv\rangle/U_\infty^2 = 0{\cdot}0005$. (*b*) Determination of x_0 from height of spot, based on temperature contours, in the plane of symmetry. ○, $\tilde{T}/\Delta T = 0{\cdot}01$; ●, 0·03; □, 0·05; △, 0·07; ▽, 0·09; ×, 0·11.

is $x_0 = 0$ and $t_0 = 0$) but such solutions did not seem to satisfy the data of figure 9 (*b*) as well as the chosen values ($x_0 = -10$ cm and $t_0 = -20$ ms). While we feel that this choice represents an adequate virtual origin for the present data, it is possible that a more accurate determination of this origin would have resulted had data been collected over a larger range of x. In I the development of the spot was monitored at several values of x_s; it was noted that it was very difficult to distinguish between a linear growth or a $x_s^{\frac{4}{5}}$ growth of the spot. While there is good evidence for the linear growth in z,† it is possible that the assumed conical growth, while perhaps convenient for the purpose of construction and analysis, may not provide the best description of flow development.

It is interesting to note that Cantwell *et al.* also obtained negative values for x_0 and t_0. In their experiment, which was conducted in a slightly favourable pressure gradient, the virtual origin was actually located upstream of the plate leading edge. Amini's (1979) plot (his figure 11) of characteristic times of front, centre and tail of his incipient

† Apart from the visual evidence, a linear spanwise growth ($\simeq 10°$) of the spot, independent of the location of the disturbance and the free-stream velocity, is produced in I.

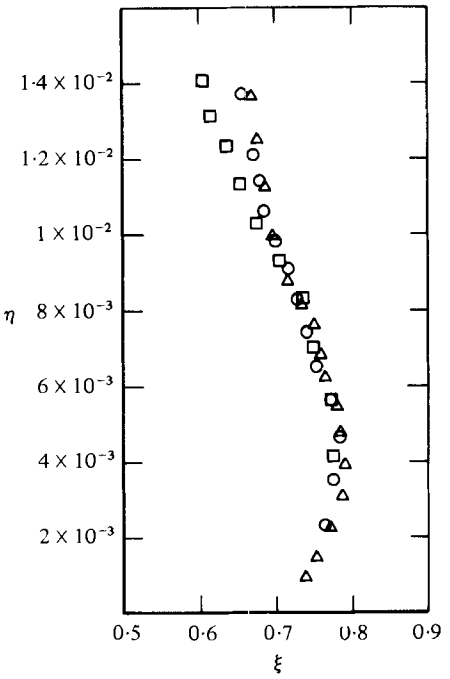

FIGURE 10. Leading-edge location in ξ, η co-ordinates. □, station 1; ○, station 2; △, station 3.

spot structure over a relatively small range of x_s (0–50 cm) indicates that the virtual origin for his incipient spot is at the location of the disturbance. Since one might expect a faster rate of growth for the laminar disturbance preceding the spot (this was observed by Cantwell *et al.*), a virtual origin at or very near the disturbance would be anticipated if only the earlier stage of spot development were used for its determination. Van Atta & Helland (1980) used arrival times for the front and back thermal interfaces of the spot at only two stations and found $x_0 = 0$, $t_0 = -12$ ms, which are not significantly different from the present values.

The slopes of the lines (or rays emanating from a virtual origin) in figure 9(*a*) represent the convection speeds of those particular features used in the construction of the ray. The convection speed of a feature along a particular ray is, of course, constant and a consequence of the assumed conical growth. Figure 9(*a*) clearly shows that the slope decreases as the T.E. of the spot is approached. The locations of the maximum $\tilde{T}$ and minimum $\tilde{U}$ contours appear to be convected at essentially the same speed. Some indication of the propagation velocity of the spot normal to the wall can be obtained by plotting loci of maximum heights of different $\tilde{T}/\Delta T$ contours as a function of time t. The locus corresponding to the maximum y location of the $\tilde{T}/\Delta T = 0{\cdot}01$ contour (this corresponds to the height h), yields a value of $\partial h/\partial t$ of $0{\cdot}014U_\infty$. This is nearly 50 times smaller than the propagation velocity in the streamwise direction. The convection speed of the L.E. (1 % $\tilde{T}$) along $\pm 3{\cdot}5°$ rays is found to be equal to $0{\cdot}59U_\infty$, which is smaller than the convection speed of $0{\cdot}74U_\infty$ along $z = 0$ (figure 9*a*). This result is in qualitative agreement with the measurements in I of the variation, in the spanwise direction, of the propagation velocity of the spot.

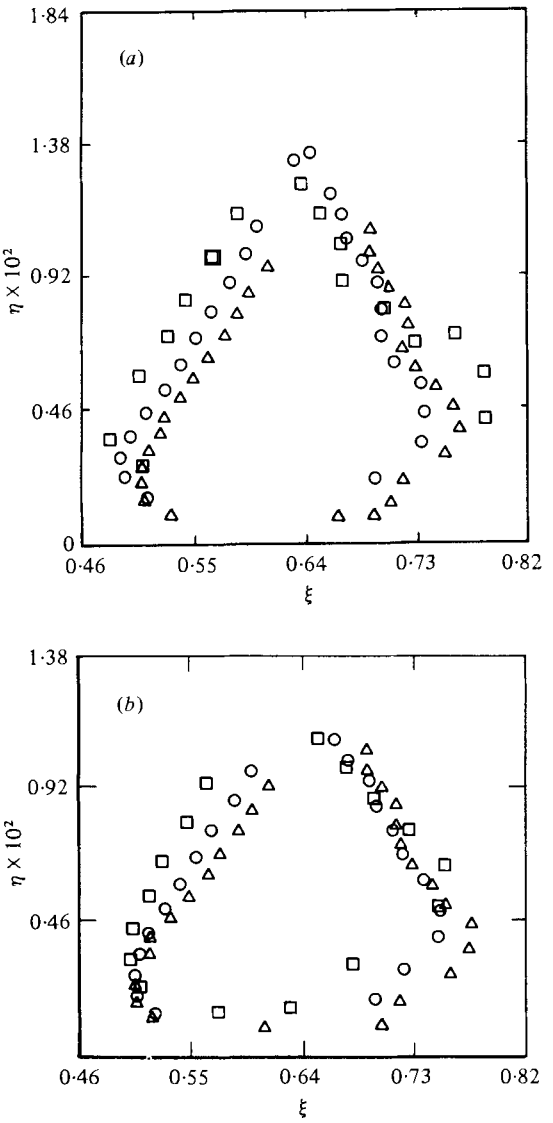

FIGURE 11(*a*, *b*). For legend see next page.

To test the conical property, the leading-edge shapes of figure 3 are re-plotted in figure 10 using ξ, η co-ordinates. The collapse is satisfactory except at the first station when η is greater than about 0·01. A test of conical similarity for $\tilde{U}$ and $\tilde{T}$ can be made by plotting, in (ξ, η) co-ordinates, contours of the velocity defect and temperature excess associated with the outer perimeter of the spot. The $\tilde{T}/\Delta T = +0{\cdot}02$ and $\tilde{U}/U_\infty = -0{\cdot}01$ contours in figures 11 (*a*) and (*b*) show only fair agreement at stations 2 and 3, and systematic differences are observed, especially toward the outer part of the T.E. These data, with the $\tilde{T}$ data of Van Atta & Helland, and the more extensive data for $\tilde{U}$ obtained by Wygnanski (private communication) indicate that the spot disturbance fields relative to laminar values do not obey conical similarity, whereas the stream function of the full centre-line velocity field, as shown by Cantwell *et al.*,

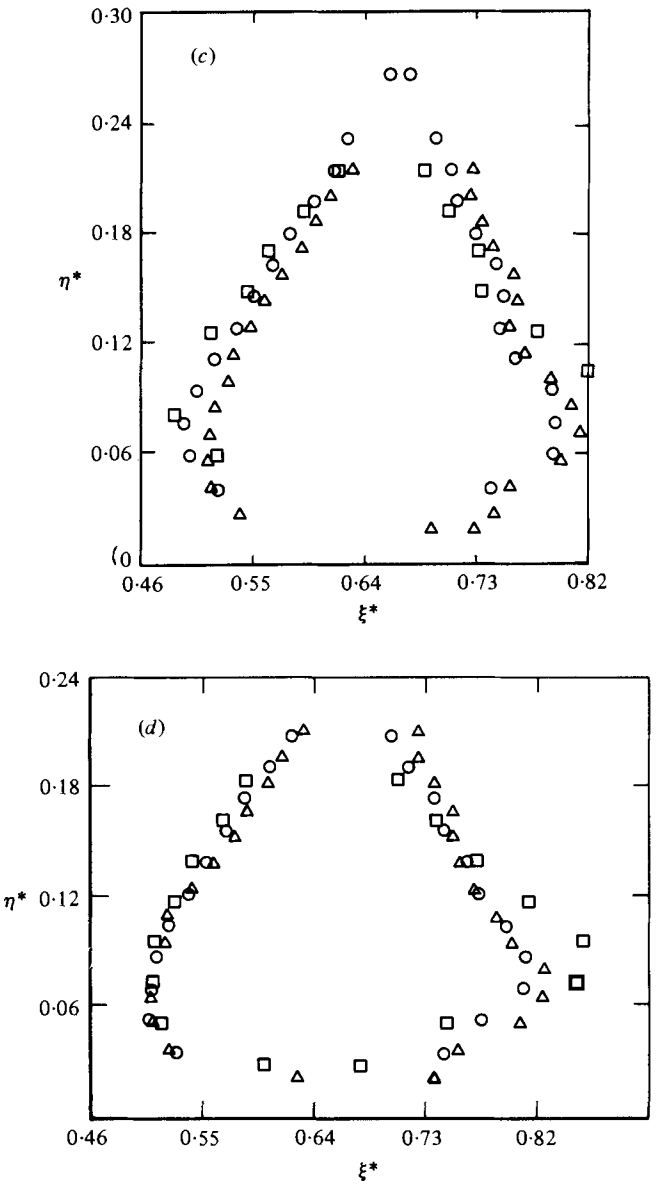

FIGURE 11. Isotemperature and velocity disturbance contours in ξ, η and ξ^*, η^* co-ordinates. (*a*) and (*c*), $\tilde{T}/\Delta T = 0{\cdot}02$; (*b*) and (*d*), $\tilde{U}/U_\infty = -0{\cdot}01$. □, station 1; ○, station 2; △, station 3.

appears consistent with a conical growth of the spot, at least to a first approximation.† We can as yet draw no definite conclusions concerning conical similarity for the full temperature field, as the lack of distinguishing features in the total temperature contours, unlike the stream function (not calculated for the present data), make accurate comparisons of data from different stations difficult.

While the disturbance contours do not exhibit conical similarity, we find that they

† Cantwell *et al.* state on p. 666 of their paper that 'the assumption of conical similarity is demonstrably not exact'.

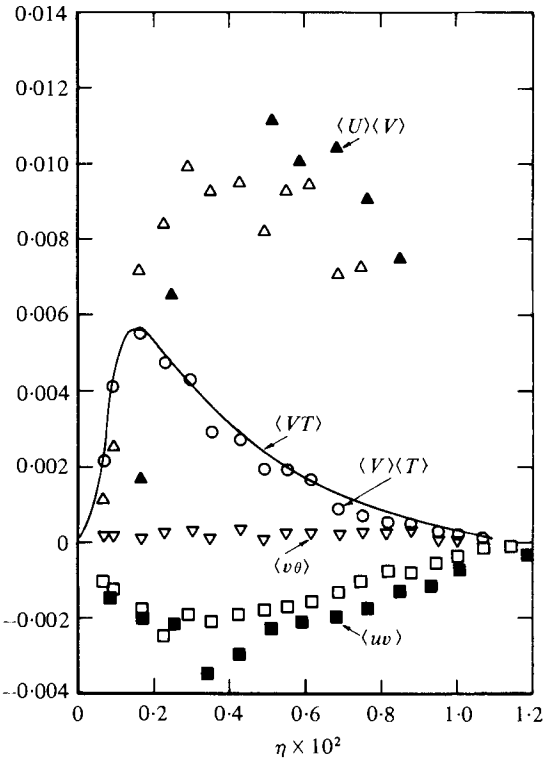

FIGURE 12. Distributions of the components $\langle UV\rangle/U_\infty^2$ and $\langle VT\rangle/U_\infty \Delta T$ at stations 2 and 3 for $\xi = 0{\cdot}62$. Open and filled-in symbols are for stations 3 and 2 respectively.

do collapse well under an alternative transformation, which applies viscous scaling to the y co-ordinate, of the type suggested independently by Wygnanski (private communication). For the present data, the transformation used was

$$\xi^* = \frac{x_s}{U_\infty(t-t_0)}, \quad \eta^* = \frac{y}{\delta(x)}, \tag{13}$$

where x_s is the distance from the spark disturbance and $\delta(x)$ expresses the growth rate of a fully turbulent boundary layer, i.e. $\delta/x = Re^{-\frac{1}{5}}$ where $Re = U_\infty x/\nu$ and x is the distance from the L.E.† of the plate.

The results of re-plotting the same data in terms of these new co-ordinates are shown in figures 11 (*c*) and (*d*). The collapse of the data represents a definite improvement over figures 11 (*a*) and (*b*). The large systematic deviations noted in conica. similarity co-ordinates have disappeared. Similar collapse was obtained for a number of other contour values of $\tilde{T}$ and $\tilde{U}$. It remains to be seen whether the alternate viscous transformation can be used to gain further insight into spot dynamics in a way similar to that achieved by Cantwell *et al.* using conical similarity for the full velocity field.

† This is strictly the origin of the laminar boundary layer but the results are not sensitive to the precise location of this origin.

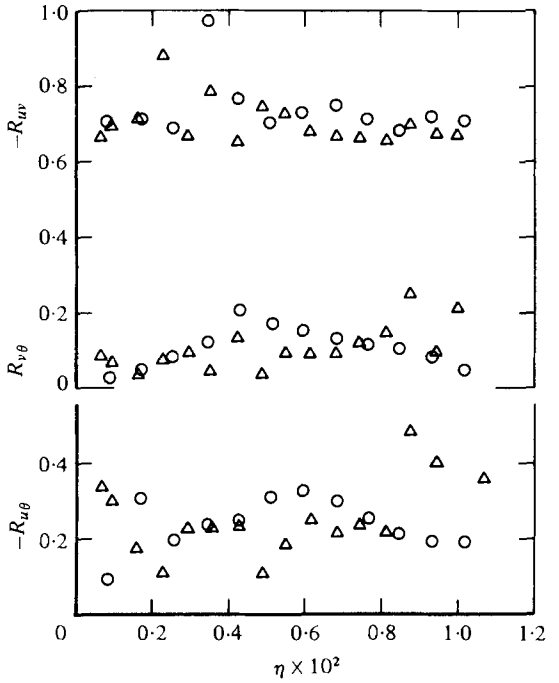

FIGURE 13. Correlation coefficients R_{uv}, $R_{v\theta}$ and $R_{u\theta}$ at $\xi = 0{\cdot}62$. ○, station 2; △, station 3.

6. Shear stress and heat flux distributions

The terms on the right-hand side of equations (7) and (9) have been calculated at stations 2 and 3 for the same value of ξ ($\simeq 0{\cdot}62$) and for different values of y (or η, since t was constant at a given station); this chosen value of time t corresponds approximately to the arrival of the maximum height of the spot at the measuring station). These terms are shown in figure 12. The magnitude of the term $\langle uv \rangle$ produced by the 'random' motion is about one third that of $\langle U \rangle \langle V \rangle$, arising from the educed coherent structure, and opposite in sign. The magnitude of $\langle v\theta \rangle$ is about one-tenth that of $\langle V \rangle \langle T \rangle$, and of the same sign. $\langle UT \rangle$ (not shown) is distributed in nearly the same way as $\langle VT \rangle$, but $\langle UT \rangle$ is about fifty times larger. The contribution of $\langle u\theta \rangle$ is negligibly small compared with that of $\langle U \rangle \langle T \rangle$.

Correlation coefficients $R_{xy} = \langle xy \rangle / x'y'$ (where x and y stand for either u, v or θ) are shown in figure 13 for stations 2 and 3 at the same value of ξ ($\simeq 0{\cdot}62$) but different values of η. The good agreement between values at the two stations follows from the observed similarity of contours of $\langle xy \rangle$ and of r.m.s. values x' and y' at those stations. To within the experimental scatter, R_{uv}, $R_{u\theta}$ and $R_{v\theta}$ are approximately constant across the spot, equal to $-0{\cdot}7$, $-0{\cdot}25$ and $+0{\cdot}1$, respectively. It is of interest to compare these values with those measured in a nearly self-preserving turbulent boundary layer over a slightly heated wall. Fulachier (1972) found that, over a major part of the layer (typically $0{\cdot}1 < y/\delta < 0{\cdot}7$, where δ is the boundary-layer thickness), $R_{v\theta} \simeq 0{\cdot}6$ whereas $R_{u\theta} \simeq -0{\cdot}5$. These values are appreciably larger than those of figure 13. The magnitude of R_{uv} in figure 13 is, on the other hand, almost twice as

large as the value of $-0{\cdot}4$ that is usually found ($0{\cdot}1 < y/\delta < 0{\cdot}7$) in a self-preserving turbulent boundary layer. Since the correlation coefficients R_{xy} refer to turbulence that rides on top of the coherent structure, it may be argued that a direct comparison between R_{xy} and the conventional correlation coefficients that are measured in a turbulent boundary layer is not justifiable. A more appropriate comparison would be between the present correlation coefficients and those that correspond to the 'background' turbulence measured relative to the educed signature of the large structure in a fully turbulent boundary layer.

7. Conclusions and final discussion

The present X-wire and cold-wire measurements obtained along the plane of symmetry of a turbulent spot indicate that the unsteady mean flow, defined on an ensemble-average basis, is only moderately well fitted by the conical growth suggested by Cantwell *et al.* The virtual origin for this conical growth, as determined (with relatively low accuracy) from data for both velocity and temperature fields, is located slightly upstream of the position of the disturbance. Isovelocity $\tilde{U}$ and isotemperature $\tilde{T}$ contours exhibit moderate agreement at the two most downstream stations when plotted in conical similarity co-ordinates. Departure from similarity at the first station would seem to confirm earlier findings that a certain development length is required before similarity is established. However, departure from similarity at this station may also reflect sensitivity to the determination of the virtual origin and to the assumed linear growth of the spot. The similarity transformation given by (13) is based on the physically plausible assumption that the vertical spreading rate of the turbulent spot is Reynolds-number dependent. This viscous transformation yields a more accurate representation of the $\tilde{U}$ and $\tilde{T}$ contours than is provided by the conical similarity transformation.

Distributions of terms that contribute to the total shear stress $\langle UV \rangle$ and total heat fluxes $\langle VT \rangle$ and $\langle UT \rangle$ suggest that the contribution $\langle U \rangle \langle V \rangle$ due to the organized motion and $\langle uv \rangle$, a quantity that is perhaps identifiable with the more conventional Reynolds shear stress in a turbulent boundary layer, are of the same order of magnitude but of opposite sign. In the case of both longitudinal and normal heat fluxes, contributions due to the organized motion are significantly larger than the contributions $\langle u\theta \rangle$ or $\langle v\theta \rangle$ arising from the background turbulence. These results seem to suggest that bulk transport of heat within the spot is relatively more effective than bulk transport of momentum.

There are noticeable differences between the mean velocity or temperature profiles across a spot and those in a turbulent boundary layer. Wygnanski *et al.* (1976) and Cantwell *et al.* (1978) have already commented on the absence of a wake-like region in the velocity distribution in the outer part of the spot. Cantwell *et al.* ascribed this absence to the vigorous motion of the primary vortex. There are also differences between the turbulence structure in a spot and that in the boundary layer. For example, the present distribution of $\langle uv \rangle$ across the spot is significantly different from that obtained in a turbulent boundary layer. Also, correlation coefficients R_{uv} and $R_{v\theta}$, which can be thought to reflect properties of the turbulence structure, are quite different in the spot than in the boundary layer. It has been noted earlier that the comparison between correlation coefficients may not be fair as it unnecessarily

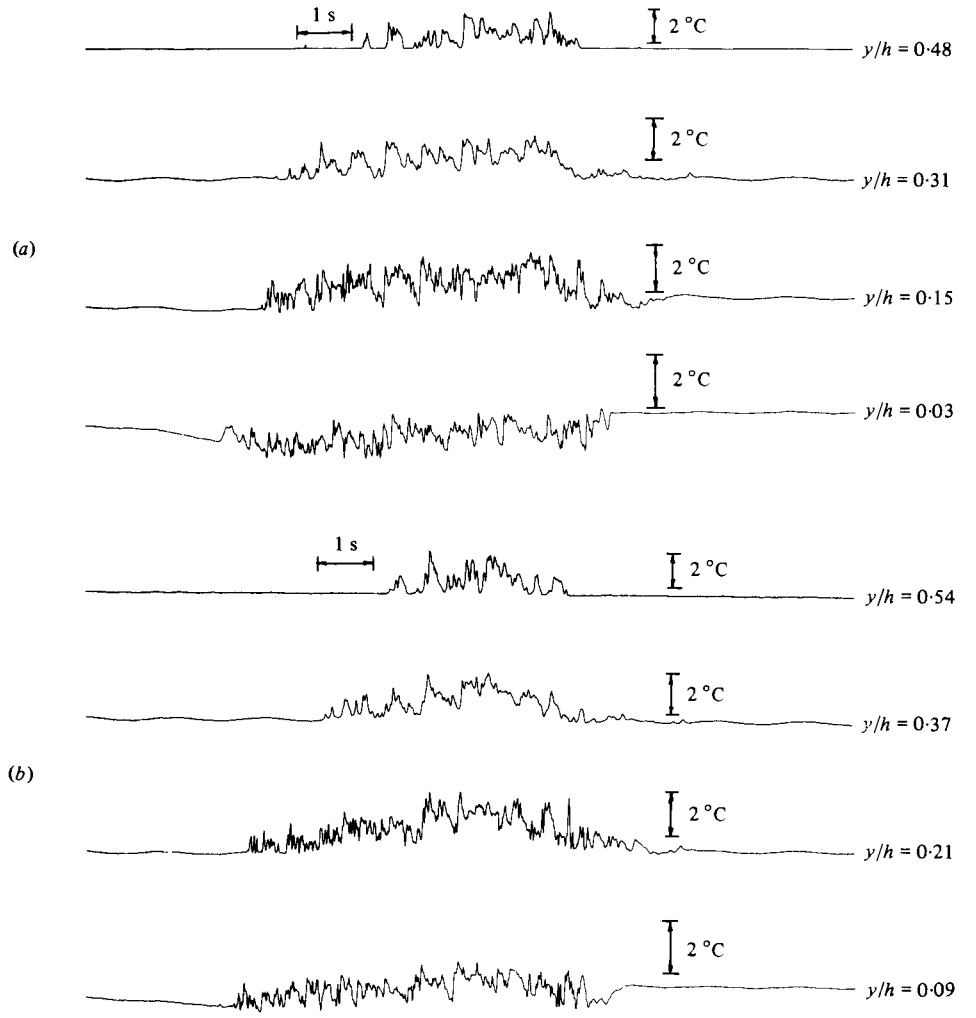

FIGURE 14(*a*, *b*). For legend see facing page.

emphasizes the importance of the background turbulence that rides over the coherent structure. The ensemble-averaged features of the spot, thought of as a large eddy, differ somewhat from those of the 'large' structure in a turbulent boundary layer. Specifically, in the outer region of the layer, measurements (e.g. Chen & Blackwelder 1978; Subramanian & Antonia 1979; Thomas & Brown 1977) of the ensemble-averaged normal velocity and temperature are positive near the back of the structure. Such a trend is not evident in the outer part of the spot.

Simultaneous temperature traces (figure 14) reveal the existence of several spatially 'coherent' structures within one spot. These structures are identified by a similar signature as is observed (e.g. traces of Chen & Blackwelder 1978) in the outer region of a turbulent boundary layer where the sharp temperature drop occurs towards the back of the 'large' structure. The boundary-layer results indicate that a relatively sharp increase in streamwise velocity is associated with this sudden decrease in temperature. Simultaneous traces observed by Wygnanski *et al.* (1979) within a spot

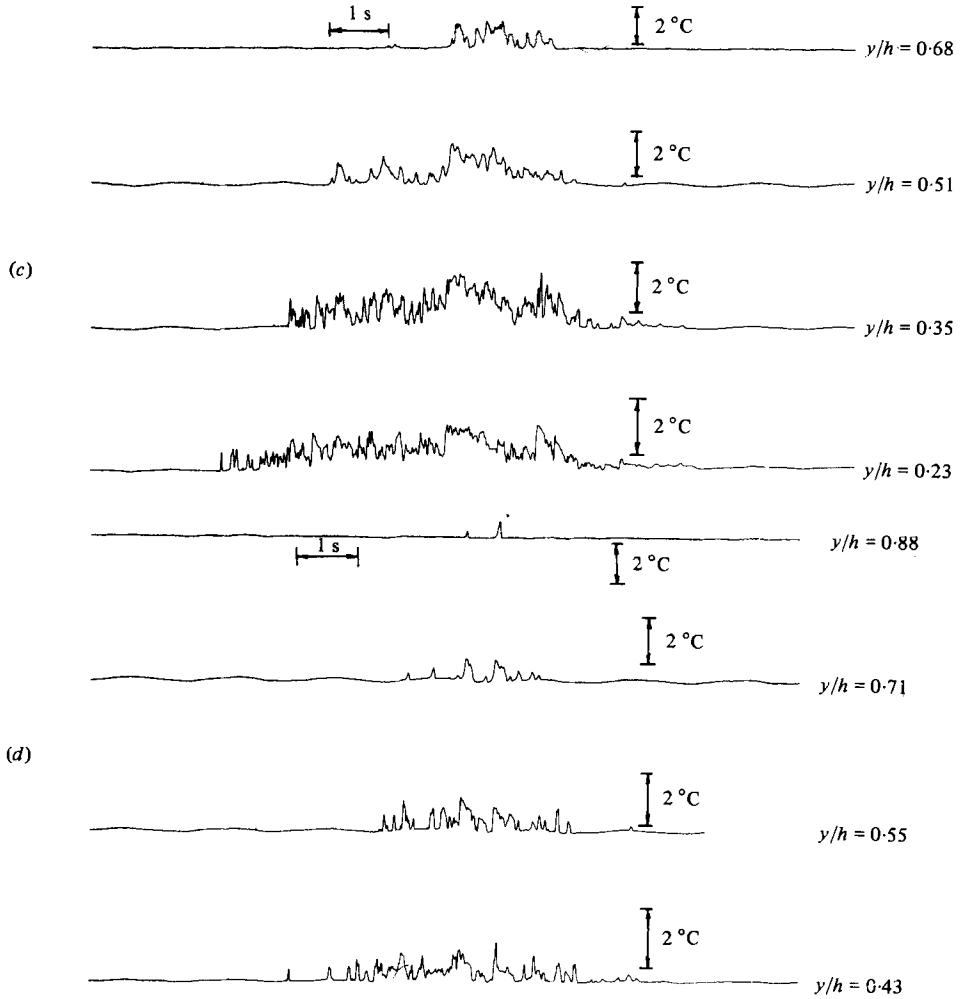

FIGURE 14. Typical simultaneous time traces of temperature from a four-wire rake at x_s = 107·2 cm ($h \simeq 2{\cdot}72$ cm). The vertical lines represent 1 °C. The horizontal line represents 0·01 s. Distance of bottom wire from plate is (*a*) 0·09 cm; (*b*) 0·26 cm; (*c*) 0·64 cm; (*d*) 1·17 cm. Time increases from right to left.

also indicate a fairly high degree of coherence in the y direction of the shear layer associated with the sharp increase in velocity. Our observations of a large number of spots indicate that these spatially coherent structures appear to occur randomly within the spot and it is therefore not surprising that their signatures are masked by the ensemble-averaging procedure outlined in § 3. It is reasonable to associate these signatures with distinct vorticity layers, similar perhaps to the hairpin vortices noted by Head & Bandyopadhyay (1978). These authors suggested that a more plausible representation of the large structure in a turbulent boundary layer is one which consists of arrays of individual vortices at a steeper angle to the surface than the upstream interface of the structure as a whole. They also observed that the upstream region of turbulent spots consists of arrays of hairpin vortices while the downstream region resembles a low-Reynolds-number turbulent boundary layer. The vorticity layers can be easily traced (e.g. figure 14*d*) to the outer edge of the spot as is the case

in a turbulent boundary layer (e.g. Chen & Blackwelder 1978). In view of the small number of wires in the array, it is difficult to say (e.g. the coherent signature is sometimes difficult to detect in the bottom trace of figure 14*a*) whether these layers bear the same phase relation to the vortical fluid in the sublayer as that suggested by Chen & Blackwelder. Such a relationship could be part of a mechanism which keeps the spot continuously energized.

R.A.A. and A.J.C. acknowledge the support of the Australian Research Grants Committee. C. W. V. A. acknowledges the support of NSF Grant ENG 78-25088.

REFERENCES

AMINI, J. 1978 Transition contrôlée en couche limite: étude expérimentale du développement d'une perturbation tridimensionelle instantanée. Ph.D. thesis, Université Scientifique et Médicale et l'Institut National Polytechnique de Grenoble.

AMINI, J. 1979 Development of a laminar spot in a transitional boundary layer. *Proc. 7th Canadian Congress Applied Mechanics, Sherbrooke*, p. 653.

BRADSHAW, P. 1971 *An Introduction to Turbulence and its Measurement.* Pergamon.

CANTWELL, B., COLES, D. & DIMOTAKIS, P. 1978 Structure and entrainment in the plane of symmetry of a turbulent spot. *J. Fluid Mech.* **87**, 641.

CHAMPAGNE, F. H. 1979 The temperature sensitivity of hot wires. In *Proc. Dynamic Flow Conf.* 1978, p. 101.

CHEN, C. P. & BLACKWELDER, R. F. 1978 Large scale motion in a turbulent boundary layer: a study using temperature contamination. *J. Fluid Mech.* **89**, 1.

COLES, D. & BARKER, S. J. 1975 Some remarks on a synthetic turbulent boundary layer. In *Turbulent Mixing in Nonreactive and Reactive Flows* (ed. S. N. B. Murthy), p. 285. Plenum.

EMMONS, H. W. 1951 The laminar–turbulent transition in a boundary layer. Part I. *J. Aero. Sci.* **18**, 490.

FIEDLER, H. 1979 On data acquisition in heated turbulent flows. *Proc. Dynamic Flow Conf.* 1978, *Skovlunde*, p. 81.

FULACHIER, L. 1972 Contribution à l'étude des analogies des champs dynamique et thermique dans une couche limite turbulente. Effet de l'aspiration. Thèse Docteur ès Sciences, Université de Provence.

HARITONIDIS, J., KAPLAN, R. E. & WYGNANSKI, I. 1978 Interaction of a turbulent spot with a turbulent boundary layer. In *Structure and Mechanisms of Turbulence II* (ed. H. Fiedler), Lecture Notes in Physics, vol. 76. Springer.

HEAD, M. R. & BANDYOPADHYAY, P. 1978 Combined flow visualization and hot-wire measurements in turbulent boundary layers. In *Coherent Structure of Turbulent Boundary Layers* (ed. C. R. Smith & D. E. Abbott), p. 98. AFOSR/Lehigh University Workshop.

HUSSAIN, A. K. M. F. & REYNOLDS, W. C. 1970 The mechanics of an organized wave in turbulent shear flow. *J. Fluid Mech.* **41**, 241.

KOVASZNAY, L. S. G., KIBENS, V. & BLACKWELDER, R. F. 1970 Large-scale motion in the intermittent region of a turbulent boundary layer. *J. Fluid Mech.* **41**, 283.

SCHLICHTING, H. 1968 *Boundary Layer Theory*, 6th edn, p. 280. McGraw-Hill.

SREENIVASAN, K. R., ANTONIA, R. A. & BRITZ, D. 1979 Local isotropy and large structures in a heated turbulent jet. *J. Fluid Mech.* **94**, 745.

SUBRAMANIAN, C. S. & ANTONIA, R. A. 1979 Some properties of the large scale structure in a slightly heated turbulent boundary layer. *Proc. 2nd Int. Symp. on Turbulent Shear Flows, London*, 4.18.

THOMAS, A. S. W. & BROWN, G. L. 1977 Large structure in a turbulent boundary layer. *Proc. 6th Australasian Hydraulics & Fluid Mechanics Conf., Adelaide*, p. 407.

VAN ATTA, C. W. & HELLAND, K. N. 1980 Exploratory temperature tagging measurements of turbulent spots in a heated laminar boundary layer. *J. Fluid Mech.* **100**, 243.

WILLMARTH, W. W. & BOGAR, T. J. 1977 Survey and new measurements of turbulent structure near the wall. *Phys. Fluids* **20**, S9.

WYGNANSKI, I. 1978 On the possible relationship between the transition process and the large coherent structures in turbulent boundary layers. In *Coherent Structure of Turbulent Boundary Layers* (ed. C. R. Smith & D. E. Abbott), p. 168. AFOSR/Lehigh University Workshop.

WYGNANSKI, I., HARITONIDIS, J. H. & KAPLAN, R. E. 1979 On a Tollmien–Schlichting wave packet produced by a turbulent spot. *J. Fluid Mech.* **92**, 505.

WYGNANSKI, I., SOKOLOV, M. & FRIEDMAN, D. 1976 On a turbulent 'spot' in a laminar boundary layer. *J. Fluid Mech.* **78**, 785.

ZILBERMAN, M., WYGNANSKI, I. & KAPLAN, R. E. 1977 Transitional boundary layer spot in a fully turbulent environment. *Phys. Fluids* **20**, S258.